

Do aqueous suspensions of smectite clays form a smectic liquid-crystalline phase?

Karin El Rifaii, Henricus Wensink, Ivan Dozov, Thomas Bizien, Laurent Michot, Jean-Christophe P. Gabriel, Josef Breu, Patrick Davidson

▶ **To cite this version:**

Karin El Rifaii, Henricus Wensink, Ivan Dozov, Thomas Bizien, Laurent Michot, et al.. Do aqueous suspensions of smectite clays form a smectic liquid-crystalline phase?. Langmuir, 2022, 38 (48), pp.14563-14573. 10.1021/acs.langmuir.2c01821 . hal-03859594

HAL Id: hal-03859594
https://hal.science/hal-03859594

Submitted on 29 Nov 2022

HAL is a multi-disciplinary open access archive for the deposit and dissemination of scientific research documents, whether they are published or not. The documents may come from teaching and research institutions in France or abroad, or from public or private research centers.

L'archive ouverte pluridisciplinaire **HAL**, est destinée au dépôt et à la diffusion de documents scientifiques de niveau recherche, publiés ou non, émanant des établissements d'enseignement et de recherche français ou étrangers, des laboratoires publics ou privés.

Do aqueous suspensions of smectite clays form a smectic liquid-crystalline phase?

Karin El Rifaii,[1] Henricus H. Wensink,[1,*] Ivan Dozov,[1] Thomas Bizien,[2] Laurent J. Michot,[3] Jean-Christophe P. Gabriel,[4] Josef Breu,[5,*] Patrick Davidson[1,*]

1 Laboratoire de Physique des Solides, Université Paris-Saclay, CNRS, 91405 Orsay, France.

2 SWING beamline, SOLEIL Synchrotron, 91192 Gif-sur-Yvette, France.

3 Laboratory of Physical Chemistry of Electrolytes and Interfacial Nanosystems (PHENIX), Sorbonne Université, CNRS, 75005 Paris, France.

4 Université Paris-Saclay, CEA,CNRS, NIMBE-LICSEN, 91191 Gif-sur-Yvette, France.

5 Bavarian Polymer Institute and Department of Chemistry, University of Bayreuth, Universitätsstrasse 30, Bayreuth, 95440, Germany.

Abstract. Bottom-up strategies for the production of well-defined nanostructures often rely on the self-assembly of anisotropic colloidal particles (nanowires, nanosheets). These building blocks can be obtained by delamination in a solvent of low-dimensionality crystallites. To optimize particle availability, determination of the delamination mechanism and the different organization stages of anisotropic particles in dispersion is essential. We address this fundamental issue by exploiting a recently developed system of fluorohectorite smectite clay mineral that delaminates in water, leading to colloidal dispersions of single-layer, very large (≈ 20 µm), clay sheets at high dilution. We show that when the clay crystallites are dispersed in water, they swell to form periodic 1-dimensional stacks of fluorohectorite sheets with very low volume fraction (< 1%) and therefore huge (≈ 100 nm) periods. Using optical microscopy and synchrotron X-ray scattering, we establish that these colloidal stacks bear strong similarities, yet subtle differences, with a smectic liquid-crystalline phase. Despite the high dilution, the colloidal stacks of sheets, called colloidal accordions, are extremely robust mechanically and can persist for years. Moreover, when subjected to AC electric fields, they rotate as solid bodies, which demonstrates their outstanding internal cohesion. Furthermore, our theoretical model captures the dependence of the stacking period on the dispersion concentration and ionic strength and explains, invoking the Donnan effect, why the colloidal accordions are kinetically stable over years, and impervious to shear and Brownian motion. Because our model is not system specific, we expect that similar colloidal accordions frequently appear as an intermediate state during the delamination process of 2-dimensional crystals in polar solvents.

INTRODUCTION

Current state of the art nanotechnology-based research relies heavily on 1- and 2-dimensional (2D) nanostructures, which gives rise to many challenges. A salient one is the development of reliable synthesis, access, and handling of such structures. Hence, many top-down or bottom-up strategies have been developed for these purposes. While top-down strategies generally depend on well-controlled depositions followed my patterned etching, using technologies developed by the semiconductor industry, bottom-up ones are more prone to use self-assembly processes of colloidal suspensions or dispersions in a solvent.[1]

Access to such colloids requires the development of exfoliation or delamination strategies of the bulk materials into their individual macromolecular constituents (nanoclusters,[2] nanowires,[3] nanotubes,[4] and nanosheets[5,6]). Then, their subsequent controlled handling and deposition must take into account, or take advantage of, their spontaneous organization into mesostructured liquid-crystalline phases.[7–9] A deep understanding of such structures, their stability and phase transitions, is therefore required to harness their full potential for applications. Hence, we report here a study on clays, which are very good model systems for 2D-nanosheet-based fluids, and allow for detailed investigations of the various stages of the delamination process.

Indeed, clay minerals enter the formulations of an extremely wide variety of industrial products in fields ranging from personal care and pharmaceutics to construction materials, oil-drilling fluids, and nanocomposites where they serve as barrier agent.[10–13] Among these minerals, the smectites family of "swelling clays", which spontaneously delaminate in polar solvents like water (when the compensating cation is monovalent), also raise particular interest from a fundamental point of view because they give rise to colloidal suspensions of nanosheets with unique properties. Indeed, as early as 1938, Irving Langmuir reported that aqueous clay suspensions can form a birefringent phase where the nanosheets have orientational order, in addition to the usual isotropic phase (Figure 1a) and in contrast with it.[14] Some sixty years later, the nature of this orientational order was compared[15] to that of lyotropic liquid crystals (LC) but the observation of an LC phase, at thermodynamic equilibrium, in suspensions of synthetic laponite and natural montmorillonite clays, was hampered by their strong tendency to form gels.[16,17] The clear-cut discovery of a nematic LC phase (Figure 1b) was only reported in 2006 when it was observed in aqueous suspensions of natural nontronite clays, a little later with beidellite clay, and more recently with synthetic hectorite and the microporous layered silicate ilerite.[18–27] Meanwhile, the smectic (i.e. lamellar) LC phase was reported for aqueous suspensions of other kinds of mineral compounds: synthetic phosphatoantimonate, niobate, and titanate nanosheets (Figure 1c).[28–30] Interestingly, the stability of the lamellar phase in these systems extends to very low concentrations, resulting in lamellar periods comparable to the wavelengths of visible light and therefore leading to photonic properties.[27,28,31,32] However, LC phases more ordered than the nematic phase, such as the lamellar or columnar LC phases, have never been clearly evidenced in clay suspensions.

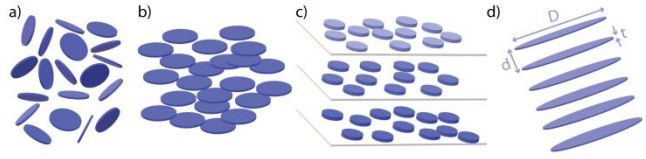


Figure 1. Schematics showing four different types of organization of colloidal suspensions of nanosheets: a) isotropic liquid; b) nematic phase; c) lamellar phase; d) 1-dimensional periodic stack. D is the average nanosheet diameter, t is their thickness, and d is the stacking period.

The ultimate defining signature of a lyotropic smectic LC phase in suspensions of clay sheets would be the presence of extremely sharp (i.e. almost resolution-limited) reflections in its X-ray scattering patterns, at small scattering angles, which corresponds to large periodicities.[29] The occurrence of a smectic phase critically depends on the perfect, thermodynamically driven, delamination of the clay lamellar crystallites in the solvent, which, in the case of synthetic clays, is best achieved when the synthesis involves a high-temperature annealing stage, leading to very large and homogeneous crystalline platelets.[22,33]

Here, we report on the observation, by polarized-light microscopy and X-ray scattering, of large birefringent domains showing periodic long-range positional order in aqueous suspensions of synthetic, high-temperature-annealed, fluorohectorite clay sheets.

We use a synthetic hectorite that has been synthesized from the melt at temperatures well above 1000 K. The material does not require any purification and shows a very homogeneous intra-crystalline reactivity while coming in appreciable crystal sizes of around 20 µm in average. With this material at hand, delamination and swelling can be studied starting with a dry powder all the way into the liquid crystalline regime simply by adding increasing amounts of water and waiting for equilibration. The obtained suspensions can be mixed with various polymers and then cast into nanocomposite coatings with superior barrier properties[34,35] as the most gentle way of delamination yields huge aspect ratios.

We then discuss and model theoretically the types of microscopic organizations (i.e. a smectic phase (Figure 1c) or 1D periodic stacks (Figure 1d)), consistent with our experimental data. We also highlight the significance of our findings in the context of the delamination process of lamellar crystallites.

RESULTS AND DISCUSSION

Visual observation of the samples

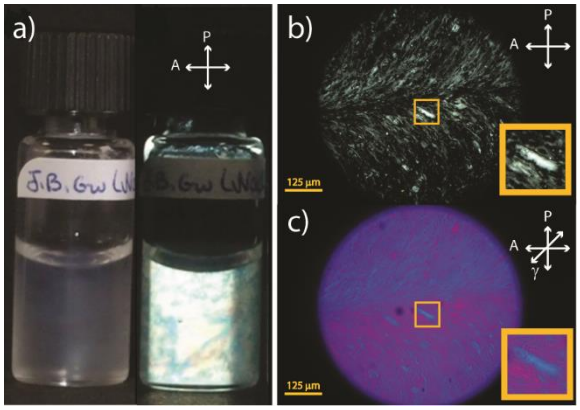


Figure 2. a) Photographs of a glass vial filled with a colloidal suspension of fluorohectorite sheets, at 1 wt% in water, observed left) in natural light and right) between crossed polarizers. b) Polarized-light microscopy image of the same colloidal suspension held in a flat glass capillary observed between crossed polarizers (white cross). The inset shows the magnified image of a "colloidal accordion" (see text). c) Image of the same sample with a wave-plate (axis γ) inserted in the light path of the microscope.

In glass vials, aqueous suspensions of fluorohectorite sheets, at concentrations between 1 and 3 wt%, appear fluid, homogeneous, and transparent in natural light (Figure 2a left), which suggests that the clay mineral powder was properly delaminated in suspension. Moreo-

ver, observation of the samples between crossed polarizers (Figure 2a right) reveals that the suspensions are birefringent liquids and are therefore in a liquid-crystalline state. At concentrations beyond 3 wt%, the suspensions form gels and therefore do not reach thermodynamic equilibrium. At lower concentrations (≈ 0.05 – 1 wt%), as expected, the suspensions spontaneously separate into a top isotropic phase and a birefringent liquid-crystalline phase, the proportion of which decreases with particle concentration. Since most of our experiments were done at an ionic strength of 10^{-4} M (NaCl), the clay sheets experience strong electrostatic repulsions and the isotropic/nematic transition is well described by the Onsager model.[36] In this respect, the present fluorohectorite clay system behaves quite like the natural clay systems previously described.[18–20] Moreover, we did not observe here any of the specific effects of gravity reported in other fluorohectorite clay systems at higher ionic strength.[26,37]

Optical microscopy

Flat glass capillaries were filled with the samples described above to examine their textures by microscopy, in natural and polarized light, with and without a wave plate (Figure 2b,c). The detailed microscopic observation of the suspensions of fluorohectorite sheets (Figure 2b) reveals that they are actually heterogeneous. Indeed, they display not only a typical liquid-crystalline nematic texture, which was already suggested by the birefringence of the samples (Figure 2a right), but also the presence of many well-defined, cylindrical, strongly birefringent domains, randomly dispersed in the nematic matrix. These objects are ca 5-50 µm in diameter, which is roughly that of the clay platelets in the powder (average size: 20 µm, Figure SI1),[24] and their length is quite variable (5 – 500 µm). Insertion of a wave plate (Figure 2c) shows that these objects are homogeneous and that their slow axis is perpendicular to their symmetry axis. Because clay nanosheets generally have their lowest refraction index along their normal,[38] we infer that, in these birefringent domains, the normals of the fluorohectorite sheets are aligned along the symmetry axis (i.e. usually their length). Moreover, these objects show no contrast at all with the nematic matrix in natural light, meaning that their light absorption and refraction properties are very close to those of the surrounding nematic liquid. In fact, they can barely be detected by phase contrast microscopy (Figure SI2). In addition, when the clay concentration in suspension decreases, these objects become smaller and less and less frequent, and the nematic matrix vanishes.

Similar colloidal objects were reported by Sayettat et al. as a transition state during delamination of the one-dimensional, inorganic phase $KPdPS_4$ in dimethylformamide, where they were described as "worm-like textures"[39], and by a Japanese team in several articles when they triggered the swelling of layered oxide crystallites of various transition metal oxides by addition of swelling agents (e.g. tetrabutylammonium hydroxide) and/or tuning the pH of the suspension.[40,41] The latter team showed that the swelling process is reversible and called these objects "colloidal accordions", terms that we will also use hereafter. Note, however, that the formation of colloidal accordions in this system of fluorohectorite clay does not require the use of an exfoliating agent, in contrast with the systems based on transition metal oxides.[40,41]

A colloidal accordion appears when a flat mineral crystallite of typically 10-100 µm diameter and several µm thickness delaminates and swells in a solvent. Because the crystallite is initially made of several thousand sheets, which all have the same diameter, and because the period of the sheet stack suddenly increases from ca 1 nm in the crystallite to ca 100 nm in suspension, the colloidal accordion length can reach up to 500 µm. Then, the broad distribution of accordion length is directly related to that of the crystalline platelet thickness in the mineral powder. We may intuitively expect that these two types of stacks, i.e. the lamellar crystallites in the powder and the colloidal accordions, because of their huge difference in volume fraction, should have very different physical properties, such as different mechanical response under stress.

All our optical microscopy and X-ray scattering data (see below) strongly suggest that the objects visible in Figure 2b,c are also colloidal accordions observed for the first time in clay minerals. Interestingly, colloidal accordions were observed in fluorohectorite sheet suspensions, independently of the conditions of sample preparation that differ greatly for optical microscopy and X-ray scattering investigations. These processes usually involve vortexing and centrifugation steps where shear deformations occur, with typical shear rates that can reach up to 10 s^{-1}, values that do not seem high enough for the colloidal accordions to crumble. Stirring samples overnight with a magnetic bar and sonicating them for 30 minutes in an ultrasound bath did not affect the colloidal accordions either. Moreover, we observed that they remained stable for at least two years. Therefore, these colloidal accordions appear remarkably robust.

X-ray scattering experiments

Our small-angle X-ray scattering (SAXS) study confirms the conclusions drawn from our observations by optical microscopy (Figure 3a,b). Indeed, the SAXS patterns of the suspensions of fluorohectorite sheets show not only the anisotropic broad peaks arising from the nematic matrix, but close inspection also reveals the presence of rows of extremely sharp equidistant reflections. Moreover, when the clay concentration in suspension decreases, the sharp reflections are less and less frequently observed, so that they very likely represent the scattering signal of the colloidal accordions. (Note that, due to their sharpness, the reflections can easily be overlooked due to the broad scattering peaks in the SAXS patterns and even more so in the azimuthally-averaged scattering curves

that are (too) commonly drawn directly from the patterns.)

Generally, the width of these reflections is comparable to that of the direct beam in both the longitudinal and transverse directions, which means that this periodic lamellar order extends over distances larger than several microns. Such X-ray scattering features are precisely those expected, both for a smectic phase (Figure 1c) and for colloidal accordions of large sheets (Figure 1d). Telling the difference between the two structures involves examining the transverse profiles of the reflections, in the perpendicular direction to the director, in order to probe the in-plane correlations between the particles, as we already discussed in a previous article.[29] Such an analysis would be impossible here because the fluorohectorite particle dimensions are too large compared to the instrumental resolution. However, the optical microscopy images only show colloidal accordions within a nematic texture, with no hint of any other phase. We therefore assign each row of sharp reflections as the scattering signal of a single colloidal accordion (in reflection conditions).

The period of the accordions decreases regularly when the overall concentration of hectorite in suspension increases (data points in Figure 6a) and when the ionic strength of the suspensions is raised (data points in Figure 6b). This latter feature strongly suggests that electrostatic repulsions between the clay particles play a major role in the formation and organization of the colloidal accordions.

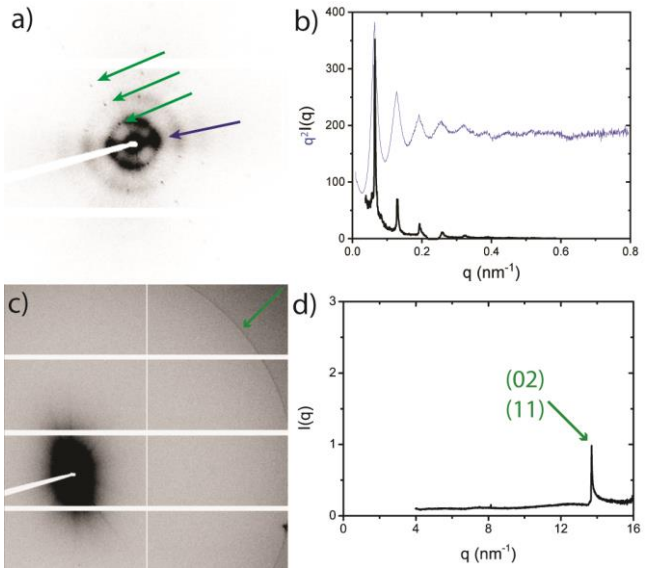


Figure 3. X-ray scattering by samples of colloidal suspensions of fluorohectorite nanosheets in water (2 wt%) a) SAXS pattern showing the sharp reflections (green arrows) from the periodic stacks and the broad scattering peaks (blue arrow) from the nematic matrix; b) Corresponding curves of azimuthally-averaged scattered intensity from the nematic matrix (blue curve) and through a row of sharp reflections (black curve); c) WAXS pattern; d) Corresponding curve of azimuthally-averaged scattered intensity I(q). In c) and d), the green arrows point to the (02)/(11) diffraction band originating from the 2D crystallinity of the individual nanosheets.

X-ray scattering measurements at wide angles (WAXS) also confirm our previous conclusions (Figure 3c,d). The WAXS patterns of the suspensions of fluorohectorite sheets only display a single sharp reflection, visible close to 14 nm^{-1}. This reflection arises from the 2D periodic structure of the individual sheets. More precisely, it corresponds to the (02)/(11) band that was already well-identified in these materials.[42] (The higher-order (hk) reflections cannot be observed in the q-range explored here.)

Electro-optical experiments

The exceptional internal cohesion of the colloidal accordions that we noted during sample preparation is quite puzzling. (By "internal cohesion", we mean that neighboring sheets in an accordion remain in register both in the longitudinal and transverse directions, despite thermal motion.) Moreover, we found that heating a sample up to 95°C had no influence on the colloidal accordions. To investigate the physical properties of the accordions in more detail we set up an electro-optical experiment to determine whether these objects could withstand a mechanical torque despite their very low sheet volume fraction ($\phi \approx 1\%$). For this purpose, we exposed the accordions to an external AC electric field (see experimental section) since we already know that the field exerts a torque on clay sheets due to the response of their counter-ion clouds, which makes them align parallel to the field.[38] Then, two kinds of behavior may be expected upon application of the field: either the individual sheets comprising the colloidal accordions rotate independently, which should destroy the accordions, or the accordions rotate as solid bodies, which will further demonstrate their internal cohesion.

The second behavior is that actually observed in our experiments (Figure 4a-d). Qualitatively, we choose, for example, a colloidal accordion lying at ca 15° with respect to the polarizer direction and looking uniformly blue with the wave plate (i.e. the clay sheets are aligned at ca 30° with respect to the wave plate slow axis.) When the electric field is applied at 45° from the polarizer and analyzer directions, the accordion rotates in a few seconds by 60°, and aligns with its main axis perpendicular to the electric field, while keeping its shape. Moreover, its color changes to orange, which shows that the clay sheets are now aligned parallel to the field direction, as expected.

The evolution with time of the angle of the accordion axis with respect to the field direction (Figure 4e) shows more quantitatively the solid-like behavior of these objects. Indeed, similar studies have previously been carried out by Itoh et al. who monitored the re-orientation in a liquid of short ceramic fibers under the influence of an electric field.[43]

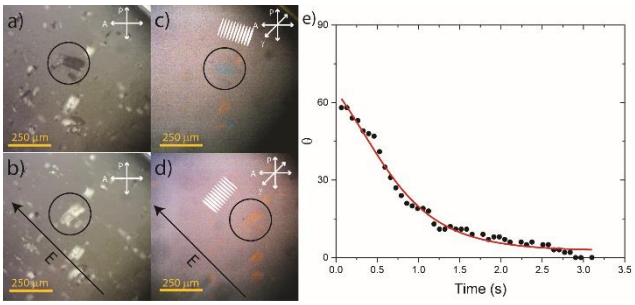


Figure 4. a-d) Polarized-light microscopy images without (a,b) and with (γ-direction in c,d) a wave-plate in zero-field (a,c) and after application of the field (black arrow in b,d) of a sample of 0.3 wt% fluorohectorite sheet suspension. e) Graph of the rotation of a colloidal accordion submitted to the electric field. The red line shows the fit of the accordion angle versus time data (black circles) by the $\tan\vartheta = \tan\vartheta_0 e^{-\frac{t}{\tau}}$ dependence discussed in the text.

The theoretical treatment of the re-orientation of an elongated (ellipsoidal) particle submitted to an electric field, neglecting inertial terms, is based on the balance of the torque exerted on the ellipsoid by the external field applied at an angle θ and the viscous torque, which leads to a differential equation of the form:

$$-\tau\left(\frac{d\vartheta}{dt}\right) = \sin\vartheta\cos\vartheta$$

where $\tau = \frac{8\pi a^3 \mu C_r}{\alpha V E_0^2}$, with a the length of the ellipsoid (i.e. the length of the colloidal accordion), μ the viscosity (Pa.s) of the solvent, C_r a constant that depends on the dimensions of the ellipsoid, α the polarizability of the particle, V its volume, and E_o the amplitude of the external electric field.[43]

The solution of this equation is of the form:

$\tan\vartheta = \tan\vartheta_0 e^{-\frac{t}{\tau}}$ with $\theta = \theta_0$ for t = 0 and Figure 4e shows that this very simple model properly fits the experimental data. The fitting parameter τ is the only one that brings interesting information on the system (i.e. the excess polarizability α of the accordion) but the viscosity μ of the nematic matrix, which is not pure solvent but has many dispersed particles in it, remains unknown. By fitting several different datasets, we always find τ in the same range: τ ≈ 0.75 s (± 0.25 s), which means that the electrical polarizability of the colloidal accordions does not vary widely. The fact that this simple model, devised for rigid rod-like particles, properly describes the electro-optical data again attests to the high internal cohesion of the colloidal accordions, in spite of their very low concentration. This very unusual behavior calls for theoretical modeling.

MESOSCALE "ACCORDIONS" OF GIGANTIC SHEETS: THEORETICAL CONSIDERATIONS

In this section, we attempt to rationalize the periodically-stacked mesostructure and stability of the stacks using a simple theoretical model based on electrostatic interactions between the sheets and on subtle ion repartitioning inside and outside the stacks. Experimental observations confirm that each colloidal "accordion" behaves as a solid body with the lateral motion of the individual sheets away from the center of the stack being severely restricted. The stacking period, d, however, may exhibit significant compression or expansion driven by changes in the ionic strength or the overall sheet concentration. With the stacking period being the principal degree of variation, the morphological response of the sheet stack thus resembles the strokes of an accordion. The purpose of our model is twofold. First, we seek to predict the stacking period and its response to changes in the sheet concentration and ionic strength. The second goal is to provide a theoretical underpinning for the remarkable co-axial stability of the accordions using first-principle kinetic arguments.

Stacking period of a colloidal accordion

Let us assume that the stack represents a perfect one-dimensional lamellar periodic structure in osmotic equilibrium with a surrounding fluid of disorganized sheets that exhibit long-ranged nematic order. The diameter of the sheets in the ambient fluid is strongly dispersed, whereas those that make up the accordion are strongly uniform in size. The space between subsequent layers is assumed to be devoid of other, smaller sheets. A sketch of the system is given in Figure 5. Following our previous work, we may contemplate a balance between van der Waals attraction and electrostatic repulsion leading to the following osmotic pressure between two charged lamellae in the colloidal accordion "A":[32,44,45]

$$\Pi_A \sim \frac{8k_BT\exp\left(\frac{-d}{\lambda_D}\right)}{\pi l_B \lambda_D^2} - 20B\frac{h^2}{d^6} \qquad (1)$$

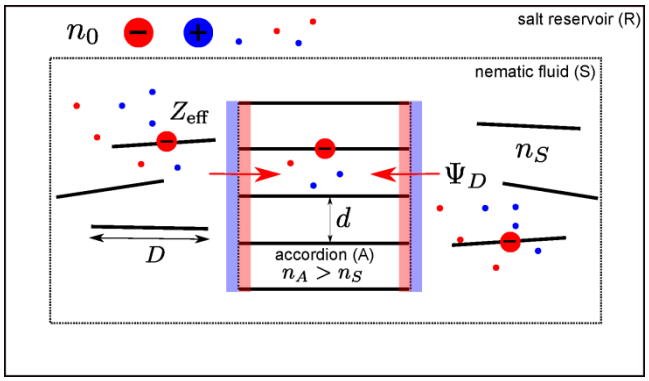


Figure 5. Cartoon summarizing the theoretical model and showing a lamellar stack ("accordion") of negatively charged sheets with effective charge Z_{eff} in osmotic equilibrium with a fluid of sheets ("S") with concentration n_S against a neutral background represented by a salt reservoir ("R"). The three compartments are separated by a semi-permeable membrane (indicated by a dotted line) that only allows co- and counterions to pass. A Gibbs-Donnan equilibrium exists between the accordion and the ambient fluid which, due to a-priori different sheet concentrations, gives rise to an electric (Donnan) potential indicated by Ψ_D.

The retarded Hamaker constant is estimated at $B \sim 10^{-28}$ J.m and the sheet thickness is $h \approx 1$ nm. The sheet surfaces are strongly charged with a Gouy-Chapman length l_{GC} = 0.22 nm, Bjerrum length $l_B \sim 0.71$ nm and a typical Debye screening length λ_D of about 30 nm.[46] We then find that the osmotic pressure exerted by the free ions within the accordion is:

$$\Pi_A \sim 308\ N/m^2 \qquad (2)$$

Note that this is the excess pressure with respect to a salt reservoir with $n_o = 10^{-4}$ M 1:1 electrolyte (corresponding to $\lambda_D \approx 30$ nm). The osmotic pressure exerted by the surrounding fluid of sheets (denoted "S") may be estimated from a simple Donnan pressure based on the assumption that the colloidal sheets do not interact with each other and constitute a uniform, structureless background, the so-called Jellium model.[47] If we further assume that the osmotic pressure is generated purely by the diffusive species (co- and counterions), we obtain the following simple expression[48,49] (a brief derivation is given in Supplementary Information/Appendix A):

$$\Pi_S = 2n_0 k_B T \left[\sqrt{\left(\frac{Zn_s}{2n_0}\right)^2 + 1} - 1 \right] \qquad (3)$$

with n_s the sheet concentration and Z the clay surface charge. The term between brackets $Zn_s/2n_o$ is the ratio of the excess counterions produced by the colloidal sheets, to the total reservoir ion concentration $2n_o$ which is responsible for the osmotic pressure. It is important to note that the sheets are strongly charged with, typically, a bare charge of about $Z_{bare} \sim 5 \times 10^8$ elementary charges per sheet[22] so that condensation of counterions at the sheet surface is expected to be quite strong. This leads to a considerable degree of charge renormalization which enables one to describe the potential around a highly charged colloid using the result from the *linearized* Poisson-Boltzmann equation, provided the bare charge is replaced by an effective one arising from an apparent constant surface potential at saturation.[44,50] Following the predictions for charge renormalization for disks,[51–53] we introduce an *effective* charge density per sheet:

$$\frac{l_B Z_{eff}}{D} \approx \frac{D}{2\lambda_D} + 1.12 \qquad (4)$$

which gives $Z_{eff} \sim 7.6$ x 10^6 charges per sheet and a surface charge density of $\sigma_{eff} \approx 0.03$ elementary charges per nm². Balancing the accordion pressure Π_A with the Donnan pressure Π_S of the colloidal sheets each with Z_{eff} charges, we may resolve the sheet packing fraction $\eta_S \approx 0.005$ which corresponds to about 1.4 wt%. This value is in good agreement with the typical sheet concentration found in experiments.

We next scrutinize the effect of varying the sheet concentration n_S and the salt concentration through $\lambda_D = 0.3/\sqrt{n_0}$ (in nm), with n_o expressed in molars. The results in Figure 6 demonstrate an expected trend, namely that increasing the sheet concentration leads to a compression of the accordions. The predicted curve is in fair agreement with the experimental data. We also observe that the stacking period is quite sensitive to changes in the salt content with a marked de-swelling observed upon increasing ionic strength (Figure 6b). Again, the match with experimental results is good which validates the predictive nature of our model at least on a qualitative level.

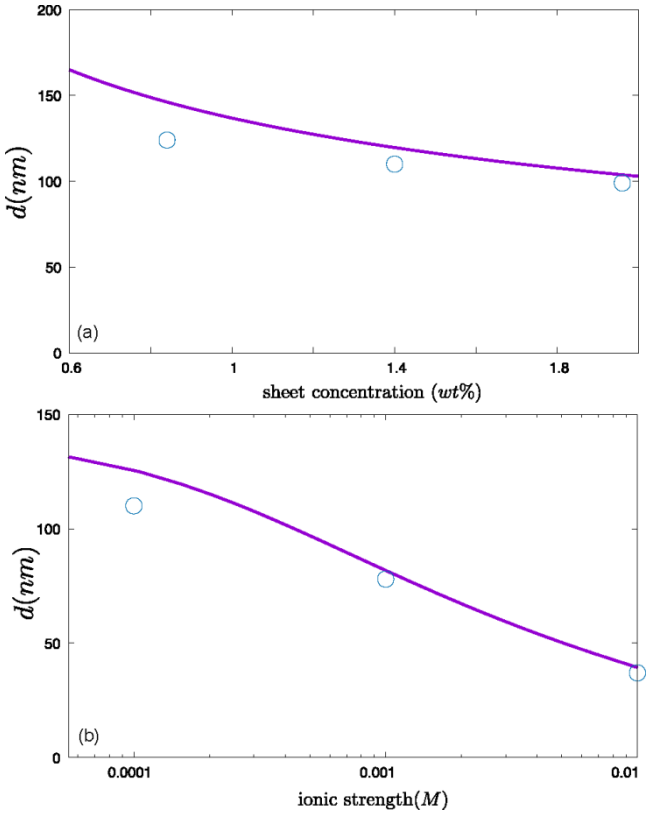


Figure 6. Variation of the lamellar distance d versus the sheet concentration (top) expressed in terms of weight percentage at fixed ionic strength n_o = 10^{-4} M and versus the salt concentration (bottom) n_o at fixed sheet concentration n_S = 1.4 wt% in the nematic matrix. Symbols represent experimental results.

Accordions as kinetically-arrested mesostacks

As established in our electro-optical experiment, the sheets within the accordion remain strongly co-axial under weak to moderate external stresses, which suggests the existence of strong restoring forces that prevent the sheets from performing lateral excursions away from the central axis. In principle, attractive van der Waals forces between the basal surfaces of adjacent sheets should counteract these displacements but their effect must be negligible in view of the steep $1/r^7$ decay of the retarded potential in Eq (1) and the large periods at hand. Alternatively, there could be strongly attractive rim-rim correlations between adjacent sheets but there is no experimental evidence supporting that these attractions should be present. For the moment, we will simply denote this restoring force by f_{res} but keep its nature unidentified. Before attempting to specify f_{res} we first provide a survey of all plausible forces acting on a single sheet that may lead to a disruption of the colloidal accordion.

Electrostatic repulsion

Sideways displacements of a clay sheet away from the stack will generally lead to a reduction of the electrostatic repulsion between adjacent sheets and are hence favored. A detailed calculation of the electrostatic displacement energy can be found in Supplementary Information/Appendix B. Combining the restoring and electrostatic forces [Eq. (S12)] we find that the displacement free energy per sheet takes a simple quadratic form:

$$\Delta F_{\rm dis} \approx f_{\rm res}\delta r - \zeta(\delta r)^2 \qquad (5)$$

with

$$\zeta = \frac{8k_BTl_BZ_{\rm eff}^2}{\pi^2 D^3}|\mathrm{F}| \qquad (6)$$

Here, F is a geometric constant of order $O(1)$ that is defined in Appendix B. It is easy to infer that the lateral displacement of a sheet implies overcoming an energy barrier ΔF_b at a critical displacement $(\delta r)_b$:

$$\Delta F_b \sim \frac{f_{\rm res}^2}{4\zeta}$$
$$(\delta r)_b \sim \frac{f_{\rm res}}{2\zeta} \qquad (7)$$

The magnitude of the restoring force is thus required to exceed a critical value $f_{res}^* >> \sqrt{4\zeta k_BT}$ for the stacks to remain kinetically stable. For large sheets with D = 18 μm at d = 120 nm for example, we find a critical force of about $f_{res}^* \sim$ 4 pN. Reducing the sheet diameter to, say D = 3 μm leads to a smaller stacking period, d = 50 nm, which requires a much larger critical restoring force $f_{res}^* \sim$ 40 pN.

Brownian motion

Next we explore the typical lateral Brownian forces acting on the sheets. For a single sheet, Brownian excursions along the face normal are deemed negligible given that the diameter largely exceeds the colloidal limit ($D >>$ 1 μm) and thermally-driven solvent-colloid collisions are far too weak to overcome the considerable solvent friction associated with dragging a gigantic sheet along the normal direction. Lateral fluctuations perpendicular to the normal, however, are expected to be much more outspoken. An estimation of the typical Brownian force requires knowing the Stokes' friction experienced by an (infinitely) flat cylinder pulled sideways through a fluid. In case of no-slip at the sheet surface, the friction factor of an infinitely thin disc with diameter D translated sideways through an unbounded fluid is $\xi = 16\,\eta D/3$.[54,55] The Brownian time scale t_B beyond which the sideways motion of the sheets should become diffusive (with average displacement $\sim\sqrt{t}$) is given by m/ξ, with m the sheet mass.[56] Some reworking gives $t_B \sim \frac{3\pi}{64} LD\rho/\eta \sim 10^{-9}$ s, with $\rho \approx 2700$ kg/m^3 the sheet mass density and $\eta \approx 10^{-3}$ Pa.s the dynamic viscosity of water. The typical time needed for a single non-interacting sheet to diffuse laterally over a

distance comparable to its diameter then follows from $t_{\text{diff}} \approx \frac{8}{3} D^3 \eta / k_B T$ which amounts to about an hour and is much less than the lifetime (more than a year) of the accordions. For comparison, for a spherical 100 nm colloid the Brownian timescale would be about a millisecond.

Shear

Finally, the accordions may be subject to shear forces due to local convection and stirring during sample preparation. The typical shear stress τ experienced by the stack may be estimated for the case when the accordion axis is aligned with the shear gradient direction. Simple shear of a Newtonian fluid then gives:

$$\tau = \eta \dot{\gamma} \tag{8}$$

Taking a typical shear rate $\dot{\gamma} \sim 10\ \text{s}^{-1}$ prevalent in experimental situations, we find:

$$f_{\text{shear}} \sim \frac{\pi}{4} D^2 \eta \dot{\gamma} \sim 3\ pN \tag{9}$$

from which we infer that $f_{\text{shear}} < f^*_{res}$ suggesting that shear forces are unlikely to disrupt the stacks.

Co-axial restoring force from Donnan potential across accordion interface

We will now attempt to identify the co-axial restoring force f_{res} by alluding to a Donnan equilibrium related to a particular repartitioning of co- and counterions distributed across the interior and exterior of the accordion. In doing so, we assume that the sheets in the accordions adopt some given *quenched* configuration (stack versus fluid matrix, see Figure 5), inherited from the delamination of the original crystallites, while the ions interspersed between the sheets remain in thermal equilibrium with a salt reservoir and are fully mobile.

As sketched in Figure 5, the accordion subsystem operates in osmotic equilibrium with a reservoir containing a nematic suspension at a packing fraction η_S. Then, the interface between the accordion and the sheet fluid around it effectively acts as a semi-permeable membrane through which ions exchange freely, whereas individual sheets cannot enter the interlayer space of the accordion from the surrounding fluid. The volume fraction inside the accordion reads $\eta_A = L/d$ which is generally higher than η_S. The different sheet concentration inside and outside the accordion gives rise to a Donnan potential Ψ_D (see Figure 5 and Appendix A):

$$\Psi_D = \frac{k_B T}{e} \operatorname{arcsinh}(y_A - y_S) \tag{10}$$

with $y_A = Z_{\text{eff}}/n_o(\pi/4)\ D^2 d)$ the excess (over reservoir) counterion concentration within the stack and $y_S = Z_{\text{eff}}\ n_S/2n_o$ the corresponding quantity for the system. For discs with D = 18 μm we find a typical Donnan potential of about $\Psi_D \approx 1.8\ k_B T/e \approx 50$ mV. This potential could be strong enough to keep the charged sheets from laterally displacing. A naive estimate of the restoring effect follows from considering that displacing a sheet away from the stack by δr involves moving $\pi D \delta r \sigma_{\text{eff}}$ charges against the Donnan voltage. The electrostatic force associated with the infinitesimal displacement reads:

$$f_{\text{res}} \sim \pi D \sigma_{\text{eff}} e \Psi_D \tag{11}$$

which gives about 12 nN for D = 18 μm sheets with an effective charge $\sigma_{\text{eff}} \sim 0.03$ elementary charges per nm². This force is several orders of magnitude larger than the critical restoring force $f^*_{res} \sim 4$ pN (which corresponds to a Donnan potential of about 0.2 mV) that is required to keep the sheet in place. Surprisingly, we find that even a minute concentration difference, $\phi_A - \phi_S$ of a few percent, which should be very hard to detect in experiment, should generate a Donnan potential that is strong enough to ensure that $f_{res} >> f^*_{res}$. The Gibbs-Donnan effect thus provides a plausible explanation for the remarkable co-axial stability of the accordions. Although the Donnan potential should disappear once local concentration of the accordion sheets equals that of the fluid nematic matrix, our model shows that a small but non-zero concentration difference is naturally enforced through equality of mechanical equilibrium $\Pi_A = \Pi_S$.

Lateral escape time of a sheet

Now that we have specified the restoring force we may estimate the typical time scale, t_{esc}, associated with a lateral escape event of a sheet within an accordion. A simple scaling form can be found by assuming the lateral escape time to be on the order of the Boltzmann factor associated with the energy barrier times the microscopic diffusion time to reach the barrier height, that is:

$$t_{\text{esc}} \sim \frac{(\delta r)_b^2}{D_L} \exp\left(\frac{\Delta F_b}{k_B T}\right) \tag{12}$$

with $D_L = k_B T/\xi$ the lateral diffusion coefficient. An overview of the results is given in Figure 7. Note that the typical escape time for a D = 18 μm sheet turns out ludicrously high, namely 10^{10^6} times the age of the universe (13.8×10^9 years)! The marked destabilization of the accordions for smaller diameters seems to agree, at least qualitatively, with experiment where no stable accordions have been found for sheet diameters less than about 3 μm. For D = 18 μm, the critical displacement $(\delta r)_b$ amounts to 20 % of the sheet diameter but drops to about 5 % for D = 3 μm sheets, indicating that small sheets need much shorter-ranged excursions to escape. From this, we infer that the co-axial stability of the accordions should be primarily attributed to their large diameter. Accordions composed of small sheets (up to a few microns) will simply dissolve into the nematic fluid that surrounds them, at least at the dilute conditions prevailing in this study.

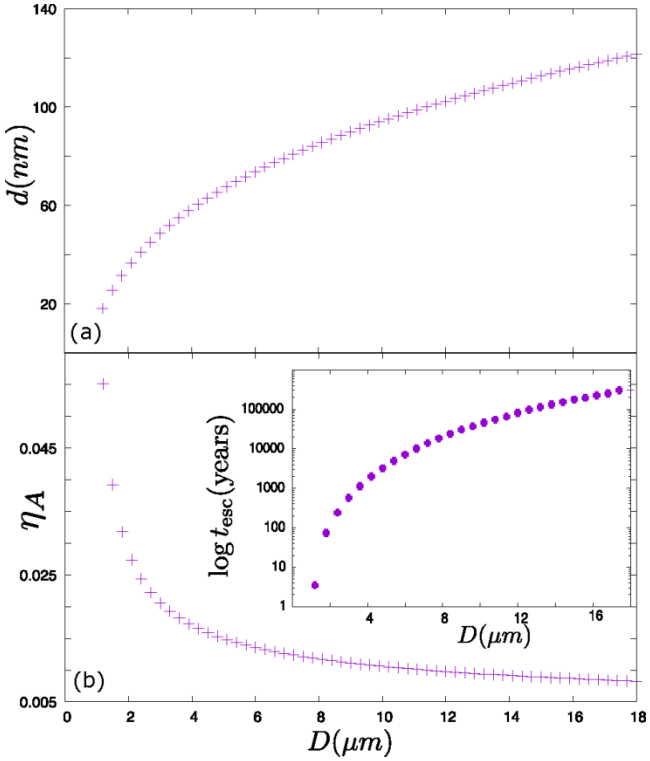


Figure 7. (a) Lamellar distance (in nm) of the accordions at constant packing fraction η_S = 0.005 of the ambient fluid, salt concentration n_o = 10^{-4} M but variable sheet diameter D (in μm). (b) Sheet packing fraction inside the accordion η_A versus D. Inset: lateral escape time of a sheet (in years) as a function of the sheet diameter. Note the double logarithmic scale on the vertical axis.

CONCLUSION

The existence of rows of very sharp peaks in the SAXS patterns of colloidal suspensions of synthetic fluorohectorite sheets is the signature of the one-dimensional periodic stacking that prevails in the colloidal accordions observed by optical microscopy. A colloidal long-range positional order has thus been identified, for the first time to our knowledge, in suspensions of clay sheets. The stacking period is about 100 nm, which is about a hundred times larger than the sheet thickness and is in good agreement with the very low (ca 1%) clay volume fraction of the suspensions. Moreover, our electro-optical study demonstrates the internal cohesion of the accordions which display a typical solid-like behavior upon application of the electric field, in spite of their low concentration, allowing for easy control of their orientation. Furthermore, the accordions show stability on the time scale of years since most of the experimental data presented in this article was acquired more than one year after sample preparation.

Our theoretical approach suggests that the colloidal accordions are only kinetically stable: they form upon the delamination of clay crystallites and do not disintegrate in the surrounding fluid due to the Donnan effect that creates an electrostatic potential barrier preventing the sideways motion of the sheets in the stack. This potential barrier strongly depends on the particle size, which explains why accordions are not observed in colloidal suspensions of small nanosheets. This mechanism also explains why the accordions are not destroyed either by the effects of Brownian motion or the shear stresses involved in sample preparation. Finally, the accordions (Figure 1d) should not be identified with a "true" lamellar liquid-crystalline phase (Figure 1c) such as the one formed by the $H_3Sb_3P_2O_{14}$ nanosheets.[29] Indeed, the notion of "phase" (in three dimensions) implies that a large number of particles are organized in a specific way in all directions of space. However, the organization of the accordions extends only over a single particle in the directions perpendicular to their stacking axis. Thus, although the accordions described in this work are a very original example of periodic organization of sheets, in our opinion, the smectic liquid-crystalline phase is still to be discovered in colloidal suspensions of smectite clays.

Finally, note that the theoretical considerations that explain the kinetic stability of the colloidal accordions do not rely on the particular features of this clay system. The only essential ingredients are the polar nature of the solvent, the presence of an electrical charge density on the sheets and of co- and counter-ions, and the large sheet diameter. Therefore, colloidal accordions may generally be expected to appear each time that large lamellar crystallites are delaminated in a polar solvent, which is a process often used to produce and handle 2-dimensional nanostructures.

EXPERIMENTAL SECTION

Fluorohectorite clay synthesis and delamination

The synthetic clay sodium fluorohectorite ($[Na_{0.5}]^{inter}[Mg_{2.5}Li_{0.5}]^{oct}[Si_4]^{tet}O_{10}F_2$) was synthesized by melt synthesis in a closed molybdenum crucible according to an already published procedure.[33] After synthesis the material was annealed for six weeks at 1045°C to improve intracrystalline reactivity, charge homogeneity and phase purity. The material featured a cation exchange capacity of 1.18 mmol g^{-1}.[57]

Fluorohectorite particle suspensions were placed in dialysis devices (Float-A-Lyzer G2, 20 kDa, Spectrum Laboratories, CA, USA) and dialyzed against a NaCl 10^{-4} M solution for five weeks to remove molecular species (meglumine delamination agent) from the dispersion. Dilution series of samples were prepared from the dialyzed suspensions, using deionized water (18 MΩ.cm).

The typical lateral extension of the clay sheets was measured with static light scattering (SLS) of an aqueous

dispersion. The number-weighted results show a relatively narrow size distribution of the particles with a mean size of about 18 µm.[33] The SLS measurements were performed in aqueous dispersions so that the particle size distribution is representative for the bulk material. As the lateral extensions obtained from SLS correlate with the hydrodynamic radius, the absolute values might be somewhat affected by the large size and the floppy nature of the sheets.

In aqueous dispersions, the fluorohectorite clay sheets bear a large negative structural electrostatic charge on their faces.[22]

Sample preparation for visual inspection, optical microscopy, and X-ray scattering

For visual inspection, all samples had the same volume of 1 ml and were poured into 2 ml glass vials equipped with Teflon-lined tight caps. All samples were prepared at the same time and were stored in the dark. The data shown in this article were recorded about 12 months (resp. 18 months) after sample preparation for X-ray scattering (resp. for sample visual observation and polarized-light microscopy). But the samples showed no slow evolution with time over more than two years.The samples were examined in natural light and between crossed polarizers to assess the dispersion state of the particles and the presence of birefringent phases.

Colloidal suspensions were filled into flat glass optical capillaries (VitroCom NJ, USA), 0.1 mm thick and 2 mm wide, for the observation of samples under the microscope. For X-ray scattering studies, the suspensions were also filled into cylindrical Lindemann glass capillaries of 1.0 ± 0.1 mm diameter (Glas-Technik & Konstruktion, Germany) and sealed with hot glue.

Optical microscopy, both in natural and polarized light, of all samples was performed with an Olympus BX51 microscope equipped with a sCMEX-20 camera (Euromex, Netherlands). A wave plate was inserted into the light path to determine the direction of the slow axis of the colloidal accordions.

A home-made, already described, setup was used to investigate the influence of an external electric field on the samples.[38] For this purpose, flat glass capillaries were placed in a plastic cell equipped with metal electrodes used to apply an AC electric voltage (1400 V_{rms}, 740 kHz) along the capillary axis. The electric field cell was placed on the stage of a Leitz polarizing microscope to monitor the influence of the electric field in real time. Videos (15 frames/s) of the alignment of colloidal accordions by the electric field were recorded using a DinoLite camera and its driving software (DinoCapture). Then, using the Irfanview software, photographs were extracted from the videos and the measurement of accordion angle versus time was performed using the ImageJ software. These data were fitted to the model described in the main text using the Mathematica software.

X-ray scattering experiments

X-ray diffraction experiments were performed at the Swing beamline of the SOLEIL synchrotron radiation facility, Saint-Aubin, France. The X-ray energy was 12 keV. For small-angle X-ray scattering (SAXS), the sample-to-detector distance, D, was 6.223 m, so that the modulus of the scattering vector, q ($q = (4\pi \sin\theta)/\lambda$ where 2θ is the scattering angle and $\lambda = 0.1033$ nm the wavelength) ranged between 0.01 and 0.8 nm^{-1} whereas for wide-angle X-ray scattering (WAXS) experiments was 0.526 m and the q-range was 1-16 nm^{-1}. The beam size was 375 x 75 μm^2 at the sample level and the scattering patterns were recorded by an Eiger-4M detector. The exposure time was typically 0.5 s. For all SAXS and WAXS experiments, the usual data reduction procedures were performed using the Swing data reduction software (Foxtrot 3.4.9) and the data were displayed either as 2D scattering patterns or as curves of scattered intensity versus scattering vector modulus, I(q), obtained by azimuthal averaging of the SAXS and WAXS patterns.

ASSOCIATED CONTENT

Scanning electron microscopy and atomic force microscopy images of fluorohectorite clay; sketch of a clay sheet with crystallographic structure; phase contrast microscopy image of colloidal accordions; polarized-light microscopy images of clay suspensions at different concentrations; theoretical description of the Donnan effect and of the energy of displacement of a clay sheet; list of parameters used in the main text. This material is available free of charge via the Internet at http://pubs.acs.org.

AUTHOR INFORMATION

Corresponding Authors

* rik.wensink@universite-paris-saclay.fr

Josef.Breu@uni-bayreuth.de

patrick.davidson@universite-paris-saclay.fr

Author Contributions

The manuscript was written through contributions of all authors. All authors have given approval to the final version of the manuscript.

Funding Sources

KER, LM, JCG, and PD acknowledge financial support from the "Agence Nationale de la Recherche" grant no. ANR-17-CE04-0003, project 4WATER.

ACKNOWLEDGMENT

We wish to thank Eric Grelet, Henk Lekkerkerker, and Tom Lubensky for helpful discussions. We acknowledge SOLEIL for provision of synchrotron radiation facilities (under the approved proposal # 20191221). We thank Florian Puchtler for synthesizing the fluorohectorite.

REFERENCES

(1) Tour, J. M. Top-Down versus Bottom-Up Fabrication of Graphene-Based Electronics. *Chem. Mater.* **2014**, *26* (1), 163–171. https://doi.org/10.1021/cm402179h.

(2) Gabriel, J.-C. P.; Boubekeur, K.; Uriel, S.; Batail, P. Chemistry of Hexanuclear Rhenium Chalcohalide Clusters. *Chem. Rev.* **2001**, *101* (7), 2037–2066. https://doi.org/10.1021/cr980058k.

(3) Tian, B.; Lieber, C. M. Nanowired Bioelectric Interfaces. *Chem. Rev.* **2019**, *119* (15), 9136–9152. https://doi.org/10.1021/acs.chemrev.8b00795.

(4) Krupke, R.; Hennrich, F.; Löhneysen, H. v.; Kappes, M. M. Separation of Metallic from Semiconducting Single-Walled Carbon Nanotubes. *Science* **2003**, *301* (5631), 344–347. https://doi.org/10.1126/science.1086534.

(5) Coleman, J. N.; Lotya, M.; O'Neill, A.; Bergin, S. D.; King, P. J.; Khan, U.; Young, K.; Gaucher, A.; De, S.; Smith, R. J.; Shvets, I. V.; Arora, S. K.; Stanton, G.; Kim, H.-Y.; Lee, K.; Kim, G. T.; Duesberg, G. S.; Hallam, T.; Boland, J. J.; Wang, J. J.; Donegan, J. F.; Grunlan, J. C.; Moriarty, G.; Shmeliov, A.; Nicholls, R. J.; Perkins, J. M.; Grieveson, E. M.; Theuwissen, K.; McComb, D. W.; Nellist, P. D.; Nicolosi, V. Two-Dimensional Nanosheets Produced by Liquid Exfoliation of Layered Materials. *Science* **2011**, *331* (6017), 568–571. https://doi.org/10.1126/science.1194975.

(6) Lv, R.; Robinson, J. A.; Schaak, R. E.; Sun, D.; Sun, Y.; Mallouk, T. E.; Terrones, M. Transition Metal Dichalcogenides and Beyond: Synthesis, Properties, and Applications of Single- and Few-Layer Nanosheets. *Accounts Chem. Res.* **2015**, *48* (1), 56–64. https://doi.org/10.1021/ar5002846.

(7) Huang, Y.; Duan, X.; Wei, Q.; Lieber, C. M. Directed Assembly of One-Dimensional Nanostructures into Functional Networks. *Science* **2001**, *291* (5504), 630–633. https://doi.org/10.1126/science.291.5504.630.

(8) Manzetti, S.; Gabriel, J.-C. P. Methods for Dispersing Carbon Nanotubes for Nanotechnology Applications: Liquid Nanocrystals, Suspensions, Polyelectrolytes, Colloids and Organization Control. *Int Nano Lett* **2019**, *9* (1), 31–49. https://doi.org/10.1007/s40089-018-0260-4.

(9) Yu, D.; Dai, L. Self-Assembled Graphene/Carbon Nanotube Hybrid Films for Supercapacitors. *J. Phys. Chem. Lett.* **2010**, *1* (2), 467–470. https://doi.org/10.1021/jz9003137.

(10) Odom, I. E. Smectite Clay Minerals: Properties and Uses. *Philosophical Transactions of the Royal Society of London. Series A, Mathematical and Physical Sciences* **1984**, *311* (1517), 391–409.

(11) Murray, H. H. Traditional and New Applications for Kaolin, Smectite, and Palygorskite: A General Overview. *Appl. Clay Sci.* **2000**, *17* (5–6), 207–221. https://doi.org/10.1016/S0169-1317(00)00016-8.

(12) Savic, I.; Stojiljkovic, S.; Savic, I.; Gajic, D. Industrial Application of Clays and Clay Minerals. *Clays and Clay Minerals: Geological Origin, Mechanical Properties and Industrial Applications; Wesley, LR, Ed* **2014**, 379–402.

(13) Choudalakis, G.; Gotsis, A. D. Permeability of Polymer/Clay Nanocomposites: A Review. *European Polymer Journal* **2009**, *45* (4), 967–984. https://doi.org/10.1016/j.eurpolymj.2009.01.027.

(14) Langmuir, I. The Role of Attractive and Repulsive Forces in the Formation of Tactoids, Thixotropic Gels, Protein Crystals and Coacervates. *J. Chem. Phys.* **1938**, *6*

(12), 873–896. https://doi.org/10.1063/1.1750183.

(15) Gabriel, J. C. P.; Sanchez, C.; Davidson, P. Observation of Nematic Liquid-Crystal Textures in Aqueous Gels of Smectite Clays. *J. Phys. Chem.* **1996**, *100* (26), 11139–11143. https://doi.org/10.1021/jp961088z.

(16) Freundlich, H. Ueber Thixotropie. *Kolloid-Zeitschrift* **1928**, *46* (4), 289–299. https://doi.org/10.1007/BF01422714.

(17) Mourchid, A.; Delville, A.; Lambard, J.; Lecolier, E.; Levitz, P. Phase-Diagram of Colloidal Dispersions of Anisotropic Charged-Particles - Equilibrium Properties, Structure, and Rheology of Laponite Suspensions. *Langmuir* **1995**, *11* (6), 1942–1950. https://doi.org/10.1021/la00006a020.

(18) Michot, L. J.; Bihannic, I.; Maddi, S.; Funari, S. S.; Baravian, C.; Levitz, P.; Davidson, P. Liquid-Crystalline Aqueous Clay Suspensions. *Proc. Natl. Acad. Sci. U. S. A.* **2006**, *103* (44), 16101–16104. https://doi.org/10.1073/pnas.0605201103.

(19) Paineau, E.; Antonova, K.; Baravian, C.; Bihannic, I.; Davidson, P.; Dozov, I.; Imperor-Clerc, M.; Levitz, P.; Madsen, A.; Meneau, F.; Michot, L. J. Liquid-Crystalline Nematic Phase in Aqueous Suspensions of a Disk-Shaped Natural Beidellite Clay. *J. Phys. Chem. B* **2009**, *113* (48), 15858–15869. https://doi.org/10.1021/jp908326y.

(20) Paineau, E.; Philippe, A. M.; Antonova, K.; Bihannic, I.; Davidson, P.; Dozov, I.; Gabriel, J. C. P.; Imperor-Clerc, M.; Levitz, P.; Meneau, F.; Michot, L. J. Liquid-Crystalline Properties of Aqueous Suspensions of Natural Clay Nanosheets. *Liq. Cryst. Rev.* **2013**, *1* (2), 110–126. https://doi.org/10.1080/21680396.2013.842130.

(21) Miyamoto, N.; Iijima, H.; Ohkubo, H.; Yamauchi, Y. Liquid Crystal Phases in the Aqueous Colloids of Size-Controlled Fluorinated Layered Clay Mineral Nanosheets. *Chem. Commun.* **2010**, *46* (23), 4166–4168. https://doi.org/10.1039/b927335b.

(22) Daab, M.; Eichstaedt, N. J.; Habel, C.; Rosenfeldt, S.; Kalo, H.; Schiessling, H.; Foerster, S.; Breu, J. Onset of Osmotic Swelling in Highly Charged Clay Minerals. *Langmuir* **2018**, *34* (28), 8215–8222. https://doi.org/10.1021/acs.langmuir.8b00492.

(23) Mayr, L.; Amschler, S.; Edenharter, A.; Dudko, V.; Kunz, R.; Rosenfeldt, S.; Breu, J. Osmotic Swelling of Sodium Hectorite in Ternary Solvent Mixtures: Nematic Liquid Crystals in Hydrophobic Media. *Langmuir* **2020**, *36* (14), 3814–3820. https://doi.org/10.1021/acs.langmuir.0c00373.

(24) Dudko, V.; Ottermann, K.; Rosenfeldt, S.; Papastavrou, G.; Breu, J. Osmotic Delamination: A Forceless Alternative for the Production of Nanosheets Now in Highly Polar and Aprotic Solvents. *Langmuir* **2021**, *37* (1), 461–468. https://doi.org/10.1021/acs.langmuir.0c03113.

(25) Hemmen, H.; Ringdal, N. I.; De Azevedo, E. N.; Engelsberg, M.; Hansen, E. L.; Méheust, Y.; Fossum, J. O.; Knudsen, K. D. The Isotropic−Nematic Interface in Suspensions of Na−Fluorohectorite Synthetic Clay. *Langmuir* **2009**, *25* (21), 12507–12515. https://doi.org/10.1021/la901784k.

(26) Ringdal, N. I.; Fonseca, D. M.; Hansen, E. L.; Hemmen, H.; Fossum, J. O. Nematic Textures in Colloidal Dispersions of Na-Fluorohectorite Synthetic Clay. *Phys. Rev. E* **2010**, *81* (4), 041702. https://doi.org/10.1103/PhysRevE.81.041702.

(27) Michels-Brito, P. H.; Dudko, V.; Wagner, D.; Markus, P.; Papastavrou, G.; Michels, L.; Breu, J.; Fossum, J. O. Bright, Noniridescent Structural Coloration from Clay Mineral Nanosheet Suspensions. *Science Advances* **2022**, *4*, eab18147. https://doi.org/10.1126/sciadv.abl8147.

(28) Gabriel, J. C. P.; Camerel, F.; Lemaire, B. J.; Desvaux, H.; Davidson, P.; Batail, P. Swollen Liquid-Crystalline Lamellar Phase Based on Extended Solid-like Sheets. *Na-*

ture **2001**, *413* (6855), 504–508. https://doi.org/10.1038/35097046.

(29) Davidson, P.; Penisson, C.; Constantin, D.; Gabriel, J.-C. P. Isotropic, Nematic, and Lamellar Phases in Colloidal Suspensions of Nanosheets. *Proc. Natl. Acad. Sci. U. S. A.* **2018**, *115* (26), 6662–6667. https://doi.org/10.1073/pnas.1802692115.

(30) Yamaguchi, D.; Miyamoto, N.; Fujita, T.; Nakato, T.; Koizumi, S.; Ohta, N.; Yagi, N.; Hashimoto, T. Aspect-Ratio-Dependent Phase Transitions and Concentration Fluctuations in Aqueous Colloidal Dispersions of Charged Platelike Particles. *Phys. Rev. E* **2012**, *85* (1), 011403. https://doi.org/10.1103/PhysRevE.85.011403.

(31) Sano, K.; Kim, Y. S.; Ishida, Y.; Ebina, Y.; Sasaki, T.; Hikima, T.; Aida, T. Photonic Water Dynamically Responsive to External Stimuli. *Nat. Commun.* **2016**, *7*, 12559. https://doi.org/10.1038/ncomms12559.

(32) El Rifaii, K.; Wensink, H. H.; Goldmann, C.; Michot, L.; Gabriel, J.-C. P.; Davidson, P. Fine Tuning the Structural Colours of Photonic Nanosheet Suspensions by Polymer Doping. *Soft Matter 17*, 9280–9292. https://doi.org/10.1039/d1sm00907a.

(33) Stöter, M.; Kunz, D. A.; Schmidt, M.; Hirsemann, D.; Kalo, H.; Putz, B.; Senker, J.; Breu, J. Nanoplatelets of Sodium Hectorite Showing Aspect Ratios of ≈20 000 and Superior Purity. *Langmuir* **2013**, *29* (4), 1280–1285. https://doi.org/10.1021/la304453h.

(34) Habel, C.; Tsurko, E. S.; Timmins, R. L.; Hutschreuther, J.; Kunz, R.; Schuchardt, D. D.; Rosenfeldt, S.; Altstädt, V.; Breu, J. Lightweight Ultra-High-Barrier Liners for Helium and Hydrogen. *ACS Nano* **2020**, *14* (6), 7018–7024. https://doi.org/10.1021/acsnano.0c01633.

(35) Röhrl, M.; Federer, L. K. S.; Timmins, R. L.; Rosenfeldt, S.; Dörres, T.; Habel, C.; Breu, J. Disorder–Order Transition—Improving the Moisture Sensitivity of Waterborne Nanocomposite Barriers. *ACS Appl. Mater. Interfaces* **2021**, *13* (40), 48101–48109. https://doi.org/10.1021/acsami.1c14246.

(36) Onsager, L. The Effects of Shape on the Interaction of Colloidal Particles. *Ann.NY Acad.Sci.* **1949**, *51* (4), 627–659. https://doi.org/10.1111/j.1749-6632.1949.tb27296.x.

(37) Fonseca, D. M.; Méheust, Y.; Fossum, J. O.; Knudsen, K. D.; Parmar, K. P. S. Phase Diagram of Polydisperse Na-Fluorohectorite--Water Suspensions: A Synchrotron Small-Angle x-Ray Scattering Study. *Phys. Rev. E* **2009**, *79* (2), 021402. https://doi.org/10.1103/PhysRevE.79.021402.

(38) Dozov, I.; Paineau, E.; Davidson, P.; Antonova, K.; Baravian, C.; Bihannic, I.; Michot, L. J. Electric-Field-Induced Perfect Anti-Nematic Order in Isotropic Aqueous Suspensions of a Natural Beidellite Clay. *J. Phys. Chem. B* **2011**, *115* (24), 7751–7765. https://doi.org/10.1021/jp201201x.

(39) Sayettat, J.; Bull, L. M.; Jobic, S.; Gabriel, J.-C. P.; Fourmigué, M.; Batail, P.; Brec, R.; Inglebert, R.-L.; Sourisseau, C. Behaviour of the One-Dimensional, Inorganic Polymer 1 ∞ [MPS 4] – Anions (M=Ni, Pd) in Organic Solutions. *Journal of Materials Chemistry* **1999**, *9* (1), 143–153. https://doi.org/10.1039/A805807E.

(40) Geng, F.; Ma, R.; Nakamura, A.; Akatsuka, K.; Ebina, Y.; Yamauchi, Y.; Miyamoto, N.; Tateyama, Y.; Sasaki, T. Unusually Stable Similar to 100-Fold Reversible and Instantaneous Swelling of Inorganic Layered Materials. *Nat. Commun.* **2013**, *4*, 1632. https://doi.org/10.1038/ncomms2641.

(41) Geng, F.; Ma, R.; Ebina, Y.; Yamauchi, Y.; Miyamoto, N.; Sasaki, T. Gigantic Swelling of Inorganic Layered Materials: A Bridge to Molecularly Thin Two-Dimensional Nanosheets. *J. Am. Chem. Soc.* **2014**, *136* (14), 5491–5500. https://doi.org/10.1021/ja501587y.

(42) Breu, J.; Seidl, W.; Stoll, A. Disorder in smectites in dependence of the interlayer cation. *Z. Anorg. Allg. Chem.* **2003**, *629* (3), 503–515. https://doi.org/10.1002/zaac.200390083.

(43) Itoh, T.; Masuda, S.; Gomi, F. Electrostatic Orientation of Ceramic Short Fibers in

Liquid. *J. Electrost.* **1994**, *32* (1), 71–89. https://doi.org/10.1016/0304-3886(94)90029-9.

(44) Verwey, E. J. W.; Overbeek, J. T. G.; Nes, K. van. *Theory of the Stability of Lyophobic Colloids: The Interaction of Sol Particles Having an Electric Double Layer*; Elsevier Publishing Company, 1948.

(45) Andelman, D. CHAPTER 12 - Electrostatic Properties of Membranes: The Poisson-Boltzmann Theory. In *Handbook of Biological Physics*; Lipowsky, R., Sackmann, E., Eds.; Structure and Dynamics of Membranes; North-Holland, 1995; Vol. 1, pp 603–642. https://doi.org/10.1016/S1383-8121(06)80005-9.

(46) Israelachvili, J. N. *Intermolecular and Surface Forces*; Academic Press, 2011.

(47) Trizac, E.; Levin, Y. Renormalized Jellium Model for Charge-Stabilized Colloidal Suspensions. *Phys. Rev. E* **2004**, *69* (3), 031403. https://doi.org/10.1103/PhysRevE.69.031403.

(48) Donnan, F. G. The Theory of Membrane Equilibria. *Chem. Rev.* **1924**, *1* (1), 73–90. https://doi.org/10.1021/cr60001a003.

(49) Philipse, A.; Vrij, A. The Donnan Equilibrium: I. On the Thermodynamic Foundation of the Donnan Equation of State. *J. Phys.-Condes. Matter* **2011**, *23* (19), 194106. https://doi.org/10.1088/0953-8984/23/19/194106.

(50) Bocquet, L.; Trizac, E.; Aubouy, M. Effective Charge Saturation in Colloidal Suspensions. *J. Chem. Phys.* **2002**, *117* (17), 8138–8152. https://doi.org/10.1063/1.1511507.

(51) Agra, R.; Trizac, E.; Bocquet, L. The Interplay between Screening Properties and Colloid Anisotropy: Towards a Reliable Pair Potential for Disc-like Charged Particles. *Eur. Phys. J. E* **2004**, *15* (4), 345–357. https://doi.org/10.1140/epje/i2004-10052-x.

(52) Alvarez, C.; Tellez, G. Screening of Charged Spheroidal Colloidal Particles. *J. Chem. Phys.* **2010**, *133* (14), 144908. https://doi.org/10.1063/1.3486558.

(53) Jabbari-Farouji, S.; Weis, J.-J.; Davidson, P.; Levitz, P.; Trizac, E. On Phase Behavior and Dynamical Signatures of Charged Colloidal Platelets. *Sci Rep* **2013**, *3*, 3559. https://doi.org/10.1038/srep03559.

(54) Sherwood, J. D. Resistance Coefficients for Stokes Flow around a Disk with a Navier Slip Condition. *Phys. Fluids* **2012**, *24* (9), 093103. https://doi.org/10.1063/1.4754869.

(55) Oberbeck, A. Ueber stationäre Flüssigkeitsbewegungen mit Berücksichtigung der inneren Reibung. In *Ueber stationäre Flüssigkeitsbewegungen mit Berücksichtigung der inneren Reibung*; De Gruyter, 2021; pp 62–80. https://doi.org/10.1515/9783112347287-003.

(56) Dhont, J. K. G. *An Introduction to Dynamics of Colloids*; Elsevier, 1996.

(57) Breu, J.; Seidl, W.; Stoll, A. J.; Lange, K. G.; Probst, T. U. Charge Homogeneity in Synthetic Fluorohectorite. *Chem. Mater.* **2001**, *13* (11), 4213–4220. https://doi.org/10.1021/cm011014m.

TOC graphic:

